# Supplementary Material

# Waste Para-rubber Wood Ash and Iron Scrap for the Sustainable Preparation of Magnetic Fenton Catalyst for Efficient Degradation of Tetracycline


Natthanan Rattanachueskul[a], Parichart Onsri[a], Waralee Watcharin[b], Arthit Makarasen[c], Supanna Techasakul[c], Decha Dechtrirat[c,d,e,*], Laemthong Chuenchom[a,f,*]

[a] *Division of Physical Science, Faculty of Science, Prince of Songkla University, Songkhla 90110, Thailand*

[b] *Faculty of Biotechnology (Agro-Industry), Assumption University, Hua Mak Campus, Bangkok 10240, Thailand*

[c] *Laboratory of Organic Synthesis, Chulabhorn Research Institute, Bangkok 10210, Thailand*

[d] *Department of Materials Science, Faculty of Science, Kasetsart University, Bangkok 10900, Thailand*

[e] *Specialized Center of Rubber and Polymer Materials for Agriculture and Industry (RPM), Faculty of Science, Kasetsart University, Bangkok 10900, Thailand*

[f] *Center of Excellence for Innovation in Chemistry, Faculty of Science, Prince of Songkla University, Songkhla 90110, Thailand*

* Corresponding author. Email address: fscidcd@ku.ac.th (D. Dechtrirat)

* Corresponding author. Email address: laemthong.c@psu.ac.th (L. Chuenchom)

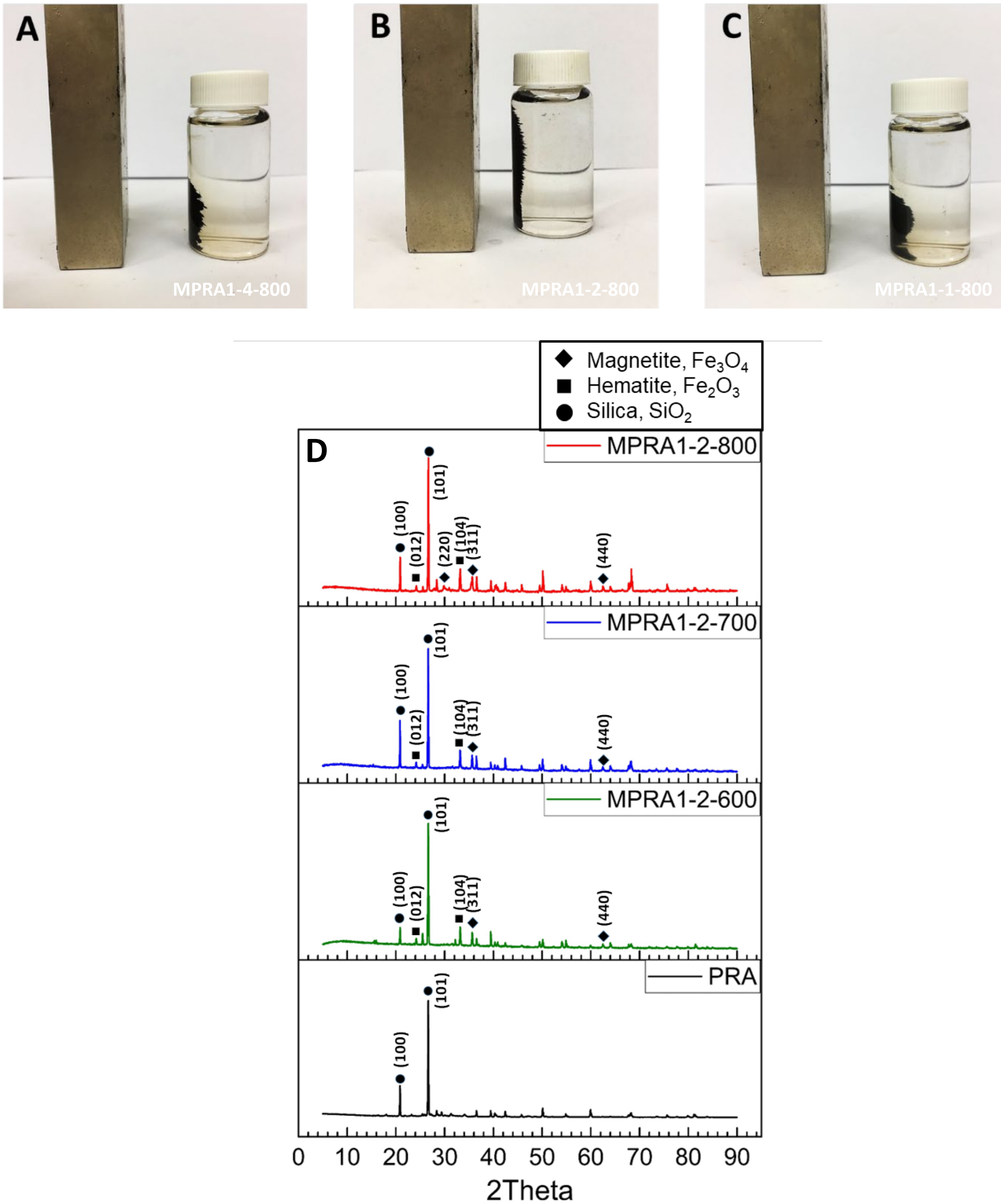


**Fig. S1** Photographs show the magnetic separation of (A) MPRA1-4-800 (B) MPRA1-2-800 and (C) MPRA1-1-800 from aqueous solution (D) XRD pattern of MPRA1-2-800, MPRA1-2-700, MPRA1-2-600, and PRA samples.

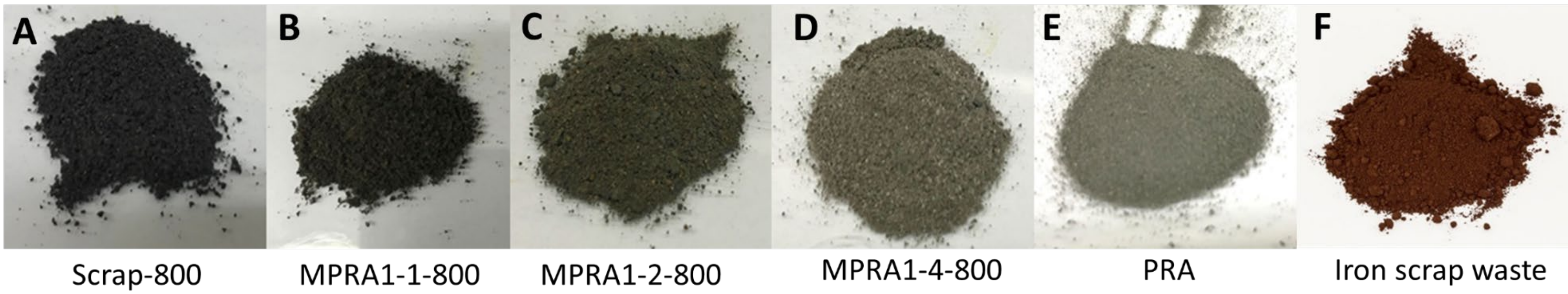


**Fig. S2** Photographs of samples

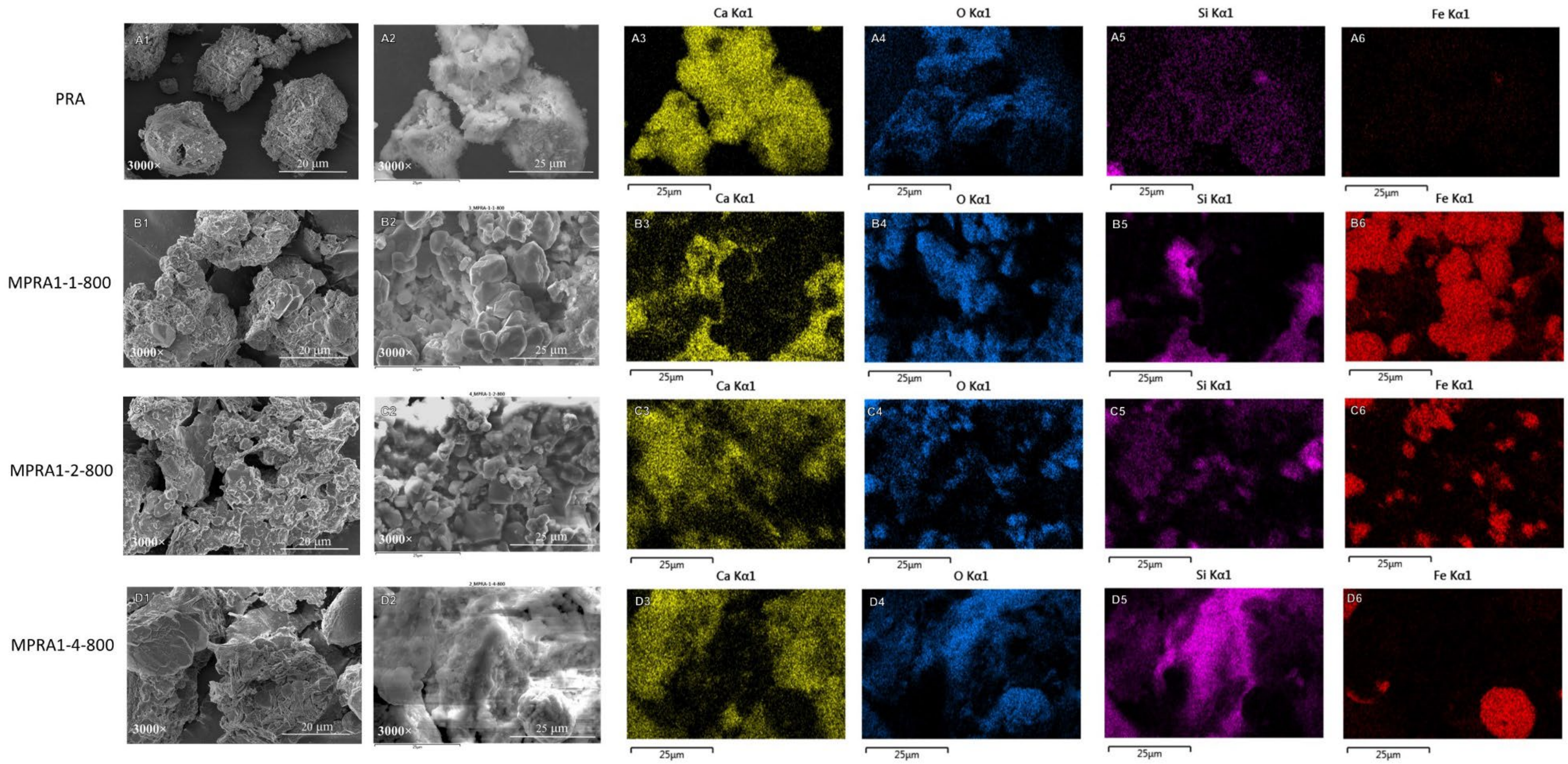


**Fig. S3** FESEM-EDX analysis. (A1 and 2) FESEM images at 3000× of PRA, (A3-A6) Elemental mapping for Ca, O, Si and Fe from (A2), (B1 and 2) FESEM images at 3000× of MPRA1-1-800, (B3-B6) Elemental mapping for Ca, O, Si and Fe from (B2), (C1 and 2) FESEM images at 3000× of MPRA1-2-800, (C3-C6) Elemental mapping for Ca, O, Si and Fe from (C2), (D1 and 2) FESEM images at 3000× MPRA1-4-800, and (D3-D6) Elemental mapping for Ca, O, Si and Fe from (D2)

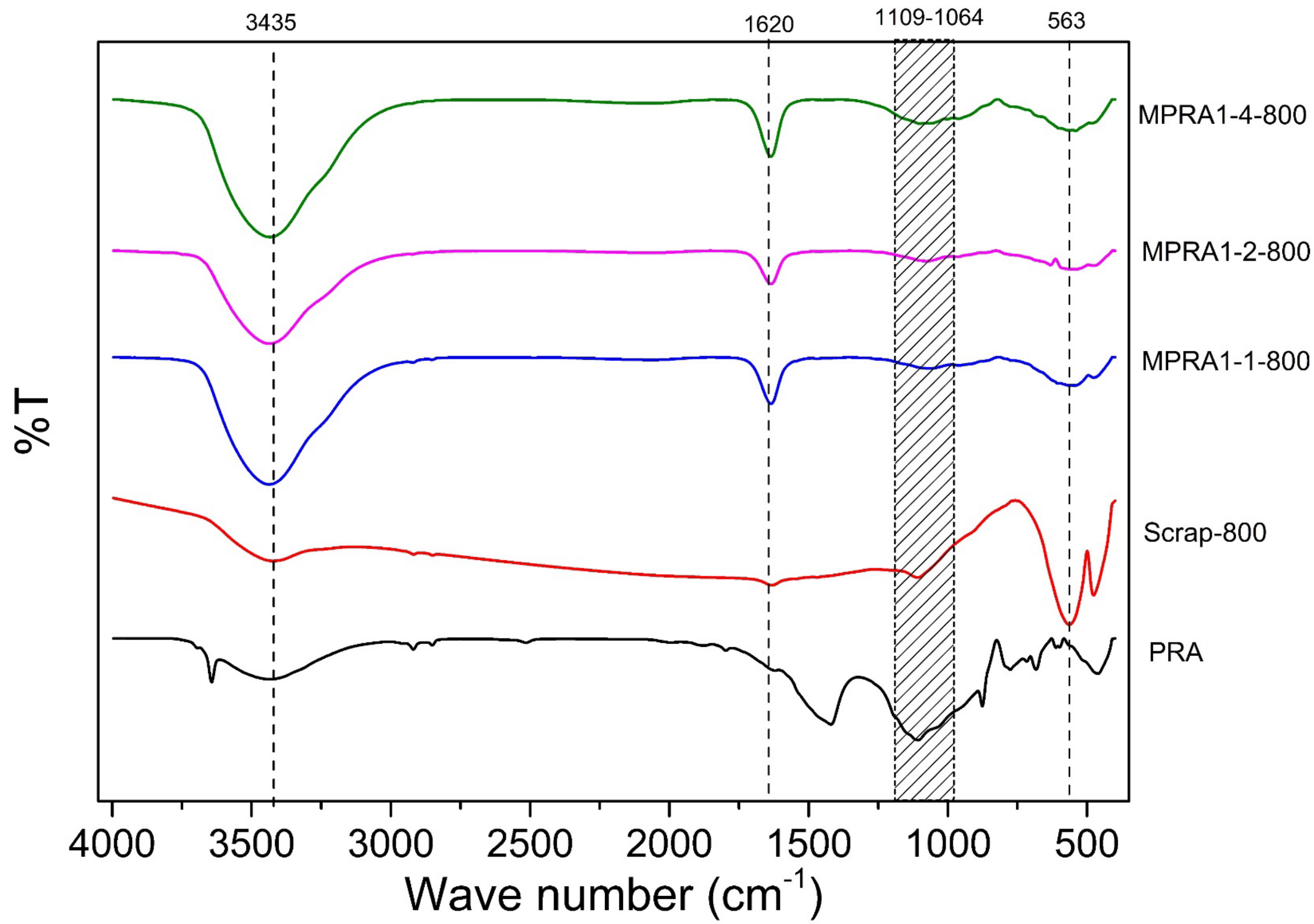


**Fig. S4** FTIR spectra of all samples

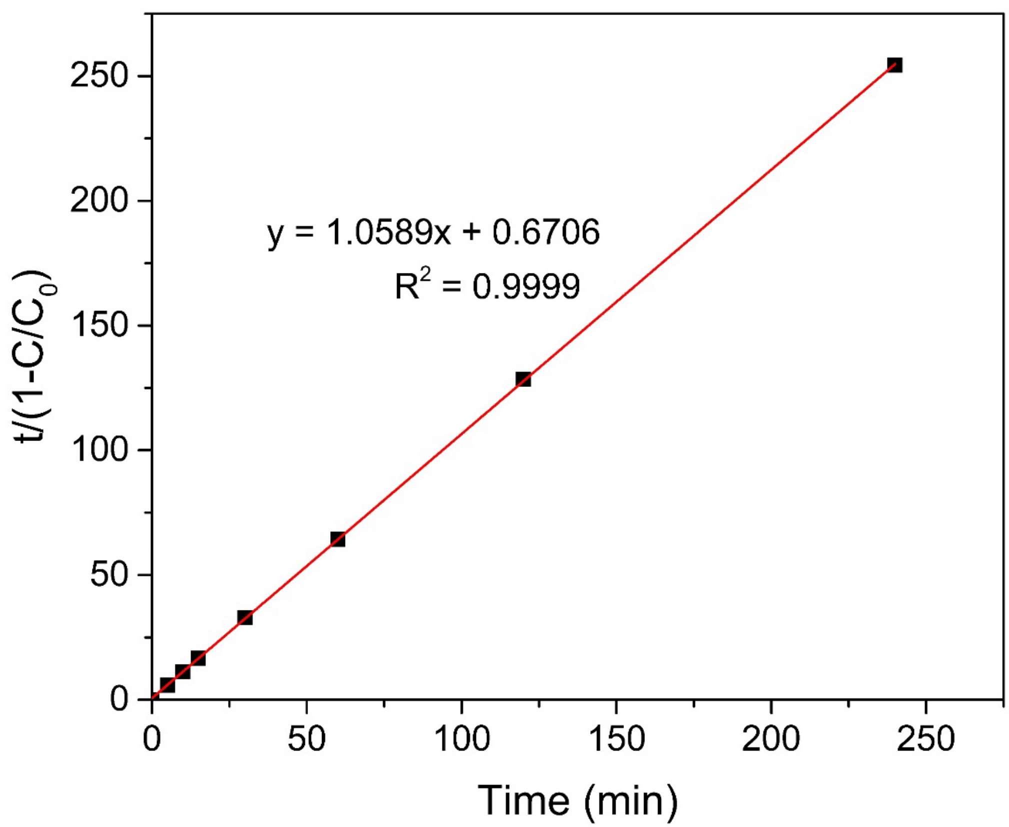


**Fig. S5** Data fitted with the BMG model for the catalytic degradation of TC on MPRA1-2-800 at pH 3.7

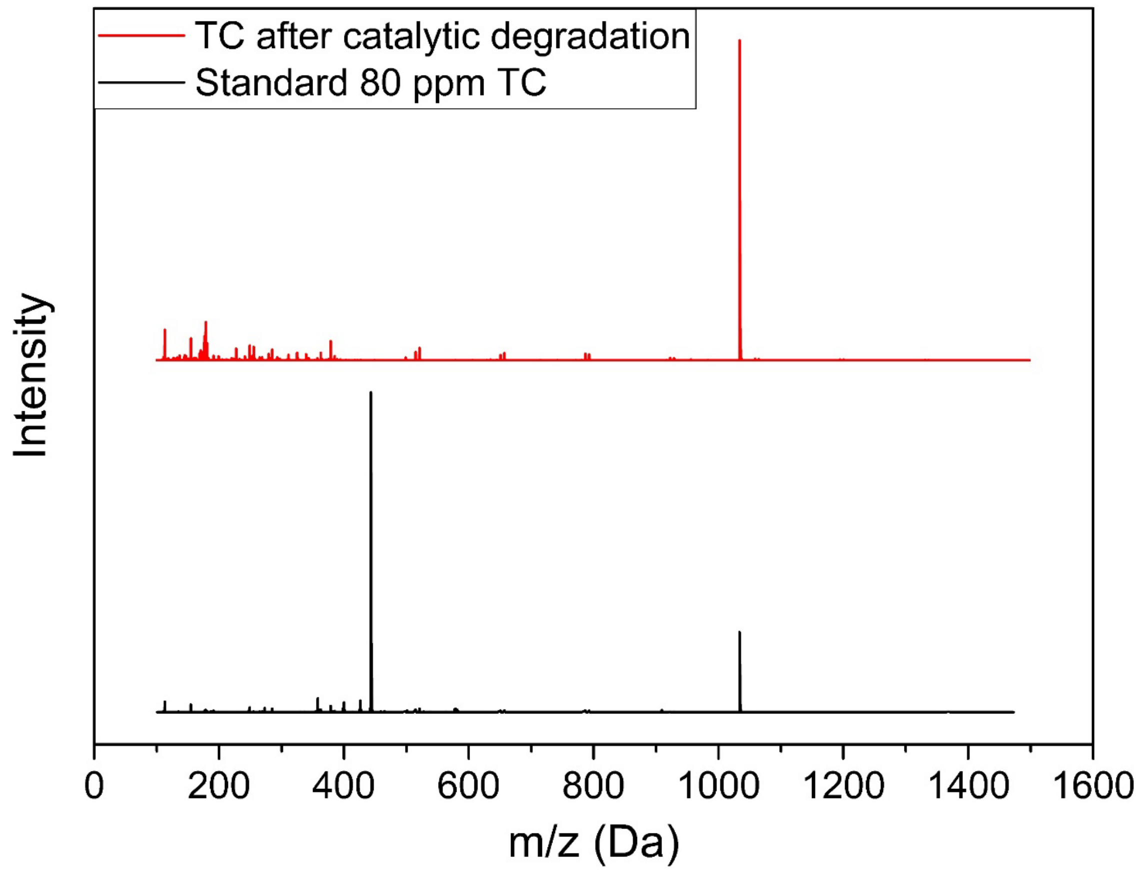


**Fig. S6** MS spectra of TC solution before and after catalytic degradation by MPRA1-2-800

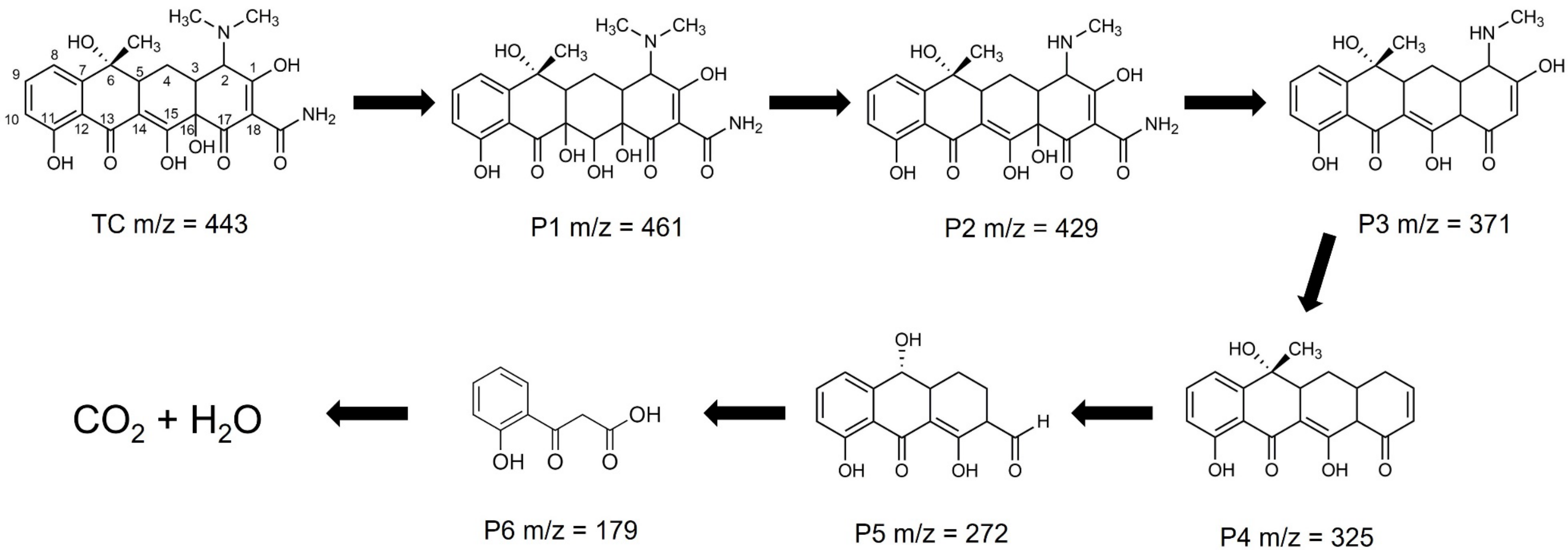


**Fig. S7** Possible mechanism for the Fenton-like degradation of TC on MPRA1-2-800

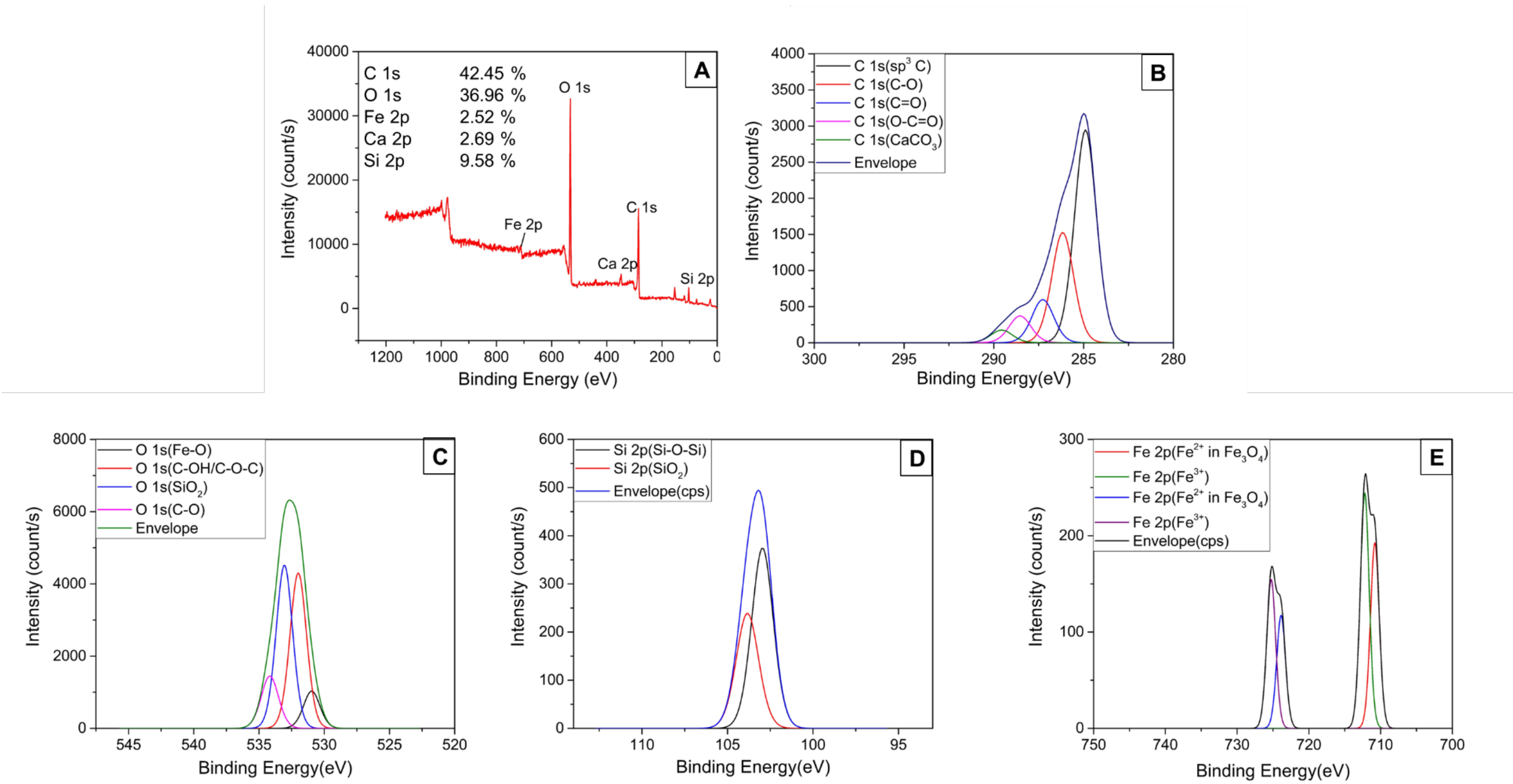


**Fig. S8** (A) The wide-scan XPS and (B-E) high-resolution C 1s, O 1s, Si 2p, and Fe 2p spectra of MPRA1-2-800 after 4 cycles of use

**Table S1** Optimization of the preparation conditions and their physical and chemical properties

| **Sample** | **Ratio of iron scrap/PRA** | **Overall Yield (%)** | **$M_s$(emu/g)** |
|---|---|---|---|
| PRA | - | - | - |
| Scrap-800 | - | 45.5±3.22 | 8.19 |
| MPRA1-1-800 | 1:1 | 49.02±2.86 | 11.08 |
| MPRA1-2-800 | 1:2 | 69.47±5.13 | 5.01 |
| MPRA1-4-800 | 1:4 | 68.57±2.81 | 0.31 |
| MPRA1-2-600 | 1:2 | 74.17±3.01 | 0.043 |
| MPRA1-2-700 | 1:2 | 70.36±2.77 | 0.11 |

**Table S2** Elemental compositions obtained from EDX spectra

| Samples | %C | SD | %O | SD | %Ca | SD | %Fe | SD | %Si | SD | %K | SD | %Cl | SD | Other |
|---|---|---|---|---|---|---|---|---|---|---|---|---|---|---|---|
| **PRA** | 11.10 | 0.70 | 44.50 | 0.40 | 16.20 | 0.10 | 1.50 | 0.00 | 12.30 | 0.10 | 5.20 | 0.10 | 2.20 | 0.00 | 7.00 |
| **MPRA1-1-800** | 13.40 | 0.30 | 27.50 | 0.20 | 4.20 | 0.00 | 43.30 | 0.20 | 6.30 | 0.10 | 1.10 | 0.00 | 2.70 | 0.00 | 1.50 |
| **MPRA1-2-800** | 15.70 | 0.40 | 32.90 | 0.20 | 6.10 | 0.10 | 14.70 | 0.10 | 8.10 | 0.10 | 6.00 | 0.10 | 14.50 | 0.10 | 2.00 |
| **MPRA1-4-800** | 14.90 | 0.40 | 39.70 | 0.20 | 8.40 | 0.10 | 6.60 | 0.10 | 15.10 | 0.10 | 2.20 | 0.00 | 10.30 | 0.10 | 2.80 |
| **Used-MPRA1-2-800** | 7.90 | 0.30 | 40.50 | 0.20 | 7.30 | 0.10 | 13.50 | 0.10 | 23.10 | 0.10 | 1.40 | 0.00 | 2.50 | 0.00 | 3.80 |

**Table S3** Assignment of the peaks in FTIR spectra of all samples

| Wave number ($cm^{-1}$) | Assignment | Structures |
|---|---|---|
| 3600-3000 | Stretching O-H | Adsorbed water and silanol group |
| 1700-1400 | Stretching C-O in carbonate groups | Calcium carbonate ($CaCO_3$) |
| | Stretching C=C | Carbon materials |
| 1109-1064 | Stretching Si-O-Si | Silicon oxide |
| 650-550 | Stretching Fe-O | Iron Oxide |

**Table S4** Assignment of the peaks in XPS analysis (C 1s, O 1s, and Fe 2p) of MPRA1-2-800

| Peak | MPRA1-2-800 BE (eV) | %Area | Peak | Used MPRA1-2-800 BE (eV) | %Area | Peak |
|---|---|---|---|---|---|---|
| C1s | 285.06 | 63.8 | $sp^3$ C | 284.9 | 52.4 | $sp^3$ C |
| | 286.38 | 17.5 | C-O | 286.17 | 27.2 | C-O |
| | 287.4 | 7.9 | C=O | 287.28 | 10.6 | C=O |
| | 288.94 | 8 | O-C=O | 288.55 | 6.6 | O-C=O |
| | 289.92 | 2.9 | $CaCO_3$ | 289.57 | 3.1 | $CaCO_3$ |
| O1s | 530.41 | 12.7 | Fe-O | 530.96 | 9.1 | Fe-O |
| | 532.04 | 63.7 | C-OH/C-O-C | 531.99 | 37.9 | C-OH/C-O-C |
| | 533.37 | 19.6 | $SiO_2$ | 533.05 | 39.7 | $SiO_2$ |
| | 534.69 | 21.5 | adsorbed $H_2O$ | 534.18 | 13.4 | C-O |
| Si 2p | 102.49 | 38.5 | silicates | 102.95 | 60.1 | Si-O-Si |
| | 103.32 | 61.5 | $SiO_2$ | 103.85 | 39.9 | $SiO_2$ |
| Fe 2p | 709.19 | 5.5 | $Fe^{2+}$ | 710.81 | 27.1 | $Fe^{2+}$ in $Fe_3O_4$ |
| | 710.66 | 17.4 | $Fe^{2+}$ in $Fe_3O_4$ | 712.22 | 34.4 | $Fe^{3+}$ |
| | 711.86 | 23.3 | $Fe^{3+}$ | 723.88 | 16.6 | $Fe^{2+}$ in $Fe_3O_4$ |
| | 713.39 | 16.5 | $Fe^{3+}$ | 725.26 | 21.9 | $Fe^{3+}$ |
| | 722.29 | 4.5 | $Fe^{2+}$ | | | |
| | 723.76 | 9.8 | $Fe^{2+}$ in $Fe_3O_4$ | | | |
| | 724.96 | 13.2 | $Fe^{3+}$ | | | |
| | 726.49 | 9.8 | $Fe^{3+}$ | | | |

**Table S5** BET surface area, pore volume and pore size for all samples

| Sample | $S_{BET}$ ($m^2$/ g) | Pore volume ($cm^3$/g) | Pore size (nm) |
|---|---|---|---|
| PRA | 1.95 | 0.005351 | 10.96 |
| Scrap-800 | 0.778 | 0.000035 | 0.18 |
| MPRA1-1-800 | 1.08 | 0.011419 | 42.29 |
| MPRA1-2-800 | 2.386 | 0.018045 | 30.25 |
| MPRA1-4-800 | 2.541 | 0.011071 | 17.43 |

**Table S6** Curated data from the literature on catalysts for TC removal and results from the current study

| Catalyst | Preparation Method | BET ($m^2/g$) | $M_s$ (emu/g) | pH | $H_2O_2$ conc. (mM) | $H_2O_2$ amount (mmol) | Catalyst loading (g/L) | T (°C) | $C_0$ (mg/L) | V (mL) | Reaction | Reaction time (min) | %Removal | TC removal (mg) | %TOC Removal | Ref. |
|---|---|---|---|---|---|---|---|---|---|---|---|---|---|---|---|---|
| $MnFe_2O_4$/bio-char composite | Co-precipitation method | 121.45 | 11.75 | 5.5 | 100 | 10 | 0.5 | 20 | 40 | 100 | Photo-Fenton Degradation | 120 | 95 | 3.80 | 37.5 | (Lai et al., 2019) |
| C−$TiO_2$ nanocomposites | Calcination and acid etching | 165.5 | - | - | - | - | 0.2 | - | 10 | 50 | Photocatalytic Degradation | 160 | 90.8 | 0.45 | - | (Ma et al., 2019) |
| $Fe_3O_4$@MSC | Co-precipitation and calcination | 120.09 | 28.71 | 7 | 10 | 2.5 | 0.5 | 23 | 50 | 250 | UV-Fenton Degradation | 40 | 99.2 | 12.40 | 72.1 | (Yu et al., 2019) |
| $Fe_3O_4$@void@$TiO_2$sphere | Sol-gel, calcination, and etching method | 101 | 28.71 | 7 | 377 | 15.08 | 0.25 | RT | 40 | 40 | UV-Fenton-like Degradation | 10 | 94 | 1.50 | 26.9 | (Du et al., 2017) |
| Fe/N−C composite | Pyrolysis at 900°C for 2 h | - | 62 | 7 | 60 | 1.5 | 0.2 | - | 100 | 25 | Ultrasound-assisted Fenton-like Degradation | 80 | 92.77 | 2.32 | 40 | (Yang et al., 2018) |
| Schorl | - | - | - | 3 | 9.9 | 0.99 | 10 | 40 | 100 | 100 | Fenton-like Degradation | 600 | 95.2 | 9.52 | 29.8 | (Zhang et al., 2018) |
| $Fe_3O_4$ nanospheres | Solvothermal at 200°C for 10 h | 25.4 | 66.8 | 7 | 50 | 1.5 | 0.5 | 25 | 40 | 30 | Fenton-like Degradation | 110 | 82 | 0.98 | 32.9 | (Nie et al., 2020) |
| NZVI/g-$C_3N_4$@EGC composite | Calcination and $KBH_4$ reduction method | 48.41 | 26.5 | 5 | - | - | 0.5 | 30 | 30 | 60 | Photo-Fenton Degradation | 120 | 99.5 | 1.79 | - | (Wang et al., 2019) |
| Fe-MOFs | Solvothermal at 110°C for 20 h | 180.41 | - | 4.1 | 98 | 9.8 | 0.1 | 14 | 50 | 100 | Photo-Fenton Degradation | 20 | 82.52 | 4.13 | 48 | (Wu et al., 2020) |
| Pal@$Fe_3O_4$ | Co-precipitation method | 69.4 | 44.11 | 7 | 100 | 10 | 0.2 | 30 | 100 | 100 | Fenton-like Degradation | 60 | 72.9 | 7.29 | - | (Lian et al., 2019) |
| $Fe_3O_4$-Cs | solvothermal at 200°C for 24 h | 20.57 | - | 3 | 10 | 2 | 0.5 | 40 | 48 | 200 | Fenton-like Degradation | 120 | 96 | 9.22 | 68.3 | (Li et al., 2020) |
| SCH/GO nanocomposites | Oxidation-co-precipitation method | 208.6 | - | 3.5 | 1 | 0.2 | 0.25 | 25 | 15 | 200 | Photo-Fenton-like Degradation | 60 | 98.3 | 2.95 | 27.3 | (Ma et al., 2020) |
| yolk-shell $ZnFe_2O_4$ | Hydrothermal method 180°C for 6 h | 83.1 | - | 2 | 20 | 2 | 0.3 | 25 | 60 | 100 | Photo-Fenton-like Degradation | 40 | 94.2 | 5.65 | - | (Xiang et al., 2020) |
| Fe/S-doped aerogel | Sol-gel and carbonization method | 222 | - | 6 | 15 | 0.3 | 1 | 25 | 10 | 20 | Fenton Degradation | 180 | 99.56 | 0.20 | 45 | (Wang et al., 2020) |
| $FeNi_3$@$SiO_2$ | Co-precipitation method | 481.58 | 69.69 | 7 | 4.4 | 0.88 | 0.5 | 20 | 20 | 200 | Fenton-like Degradation | 180 | 87 | 3.48 | - | (Khodadadi et al., 2019) |
| Pyrite | Natural resource | 11.61 | - | 4 | 5 | 0.25 | 1 | 25 | 50 | 50 | Fenton-like Degradation | 30 | 85 | 2.13 | 62 | (Mashayekh-Salehi et al., 2021) |
| C@FONC | Coprecipitation method | - | 23.1 | 3 | 5 | 2.5 | 0.5 | 40 | 150 | 500 | Fenton-like Degradation | 120 | 97 | 72.75 | 52.7 | (Zhou et al., 2020) |
| $CuFeO_2$/BC | Pyrolysis at 450°C for 2 h, hydrothermal method 180°C for 24 h | 37.3 | 0.084 | 5 | 50 | 5 | 0.5 | 25 | 20 | 100 | Fenton-like Degradation | 300 | 89 | 1.78 | 58.5 | (Xin et al., 2021) |
| Fe-MPC | Pyrolysis at 500°C for 2 h | 33.49 | - | 4.3 | 1 | 0.05 | 0.02 | 25 | 40 | 50 | Fenton-like Degradation | 10 | 83 | 1.66 | - | (Wang et al., 2021) |
| $Fe_3O_4$@SC nanocomposites | Ball milled followed by pyrolysis at 800°C for 2 h | 386.2 | 52.2 | 5.0 | 5 | 0.15 | 0.8 | 25 | 20 | 30 | Photo-Fenton-like Degradation | 35 | 98.2 | 0.59 | 79.5 | (Wu et al., 2024) |
| *MPRA1-2-800* | *Pyrolysis at 800°C for 1.5 h* | *2.39* | *5.01* | *3.7* | *5* | *1* | *1* | *28* | *80* | *200* | *Fenton-like Degradation* | *240* | *95.61* | *15.30* | *90.81* | *This work* |

## References

Du, D., Shi, W., Wang, L., Zhang, J. 2017. Yolk-shell structured $Fe_3O_4$@void@$TiO_2$ as a photo-Fenton-like catalyst for the extremely efficient elimination of tetracycline. Appl. Catal. B: Environ. **200**, 484-492.

Khodadadi, M., Hossein Panahi, A., Al-Musawi, T.J., Ehrampoush, M.H., Mahvi, A.H. 2019. The catalytic activity of $FeNi_3$@$SiO_2$ magnetic nanoparticles for the degradation of tetracycline in the heterogeneous Fenton-like treatment method. J. Water Proc.engineering. **32**, 100943.

Lai, C., Huang, F., Zeng, G., Huang, D., Qin, L., Cheng, M., Zhang, C., Li, B., Yi, H., Liu, S., Li, L., Chen, L. 2019. Fabrication of novel magnetic $MnFe_2O_4$/bio-char composite and heterogeneous photo-Fenton degradation of tetracycline in near neutral pH. Chemosphere. **224**, 910-921.

Li, X., Cui, K., Guo, Z., Yang, T., Cao, Y., Xiang, Y., Chen, H., Xi, M. 2020. Heterogeneous Fenton-like degradation of tetracyclines using porous magnetic chitosan microspheres as an efficient catalyst compared with two preparation methods. Chem. Eng. J. **379**, 122324.

Lian, J., Ouyang, Q., Tsang, P.E., Fang, Z. 2019. Fenton-like catalytic degradation of tetracycline by magnetic palygorskite nanoparticles prepared from steel pickling waste liquor. Appl. Clay Sci. **182**, 105273.

Ma, S., Gu, J., Han, Y., Gao, Y., Zong, Y., Ye, Z., Xue, J. 2019. Facile Fabrication of C–$TiO_2$ nanocomposites with enhanced photocatalytic activity for degradation of tetracycline. ACS Omega. **4**(25), 21063-21071.

Ma, S., Jing, J., Liu, P., Li, Z., Jin, W., Xie, B., Zhao, Y. 2020. High selectivity and effectiveness for removal of tetracycline and its related drug resistance in food wastewater through schwertmannite/graphene oxide catalyzed photo-Fenton-like oxidation. J. Hazard. Mater. **392**, 122437.

Mashayekh-Salehi, A., Akbarmojeni, K., Roudbari, A., Peter van der Hoek, J., Nabizadeh, R., Dehghani, M.H., Yaghmaeian, K. 2021. Use of mine waste for $H_2O_2$-assisted heterogeneous Fenton-like degradation of tetracycline by natural pyrite nanoparticles: Catalyst characterization, degradation mechanism, operational parameters and cytotoxicity assessment. J. Clean. Prod. **291**, 125235.

Nie, M., Li, Y., He, J., Xie, C., Wu, Z., Sun, B., Zhang, K., Kong, L., Liu, J. 2020. Degradation of tetracycline in water using $Fe_3O_4$ nanospheres as Fenton-like catalysts: kinetics, mechanisms and pathways. New J. Chem. **44**(7), 2847-2857.

Wang, C., Sun, R., Huang, R., Wang, H. 2021. Superior fenton-like degradation of tetracycline by iron loaded graphitic carbon derived from microplastics: Synthesis, catalytic performance, and mechanism. Sep. Purif. Technol. **270**, 118773.

Wang, X., Xie, Y., Ma, J., Ning, P. 2019. Facile assembly of novel g-$C_3N_4$@expanded graphite and surface loading of nano zero-valent iron for enhanced synergistic degradation of tetracycline. RSC Adv. **9**(59), 34658-34670.

Wang, X., Zhuang, Y., Zhang, J., Song, L., Shi, B. 2020. Pollutant degradation behaviors in a heterogeneous Fenton system through Fe/S-doped aerogel. Sci. Total Environ. **714**, 136436.

Wu, C., Guo, T., Chen, Y., Tian, Q., Zhang, Y., Huang, Z., Hu, H., Gan, T. 2024. Facile synthesis of excellent $Fe_3O_4$@starch-derived carbon Photo-Fenton catalyst for tetracycline degradation: Rapid $Fe^{3+}/Fe^{2+}$ circulation under visible light condition. Sep. Purif. Technol. **329**, 125174.

Wu, Q., Yang, H., Kang, L., Gao, Z., Ren, F. 2020. Fe-based metal-organic frameworks as Fenton-like catalysts for highly efficient degradation of tetracycline hydrochloride over a wide pH range: Acceleration of Fe(II)/ Fe(III) cycle under visible light irradiation. Appl. Catal. B: Environ. **263**, 118282.

Xiang, Y., Huang, Y., Xiao, B., Wu, X., Zhang, G. 2020. Magnetic yolk-shell structure of $ZnFe_2O_4$ nanoparticles for enhanced visible light photo-Fenton degradation towards antibiotics and mechanism study. Appl. Surf. Sci. **513**, 145820.

Xin, S., Liu, G., Ma, X., Gong, J., Ma, B., Yan, Q., Chen, Q., Ma, D., Zhang, G., Gao, M., Xin, Y. 2021. High efficiency heterogeneous Fenton-like catalyst biochar modified $CuFeO_2$ for the degradation of tetracycline: Economical synthesis, catalytic performance and mechanism. Appl. Catal. B: Environ. **280**, 119386.

Yang, Y., Zhang, X., Chen, Q., Li, S., Chai, H., Huang, Y. 2018. Ultrasound-assisted removal of tetracycline by a Fe/N–C Hybrids/$H_2O_2$ Fenton-like system. ACS Omega. **3**(11), 15870-15878.

Yu, X., Lin, X., Li, W., Feng, W. 2019. Effective removal of tetracycline by using biochar supported $Fe_3O_4$ as a UV-Fenton catalyst. *C* Chem. Res. Chin. Univ. **35**(1), 79-84.

Zhang, Y., Shi, J., Xu, Z., Chen, Y., Song, D. 2018. Degradation of tetracycline in a schorl/$H_2O_2$ system: Proposed mechanism and intermediates. Chemosphere. **202**, 661-668.

Zhou, J., Ma, F., Guo, H., Su, D. 2020. Activate hydrogen peroxide for efficient tetracycline degradation via a facile assembled carbon-based composite: Synergism of powdered activated carbon and ferroferric oxide nanocatalyst. Appl. Catal. B: Environ. **269**, 118784.